Published in final edited form as:

NMR Biomed. 2014 December ; 27(12): 1439–1450. doi:10.1002/nbm.3227.

Vertical Gradients in Regional Alveolar Oxygen Tension in Supine Human Lung Imaged by Hyperpolarized ^{3}He MRI

Hooman Hamedani[1], **Hoora Shaghaghi**[1], **Stephen J. Kadlecek**[1], **Yi Xin**[1], **Biao Han**[1], **Sarmad Siddiqui**[1], **Jennia Rajaei**[1], **Masaru Ishii**[2], **Milton Rossman**[3], and **Rahim R. Rizi**[1]

[1]Department of Radiology, University of Pennsylvania, Philadelphia, PA, United States

[2]Departments of Otolaryngology-Head and Neck Surgery, Johns Hopkins University, Baltimore, MD, United States

[3]Department of Pulmonary and Critical Care, Johns Hopkins University of Pennsylvania, Philadelphia, PA, Baltimore, MD, United States

Abstract

Purpose—To evaluate whether regional alveolar oxygen tension (P_AO_2) vertical gradients imaged with hyperpolarized ^{3}He can identify smoking-induced pulmonary alterations. To compare these gradients with common clinical measurements including pulmonary function tests, the six minute walk test, and the St. George's Respiratory Questionnaire.

Materials and Methods—8 healthy nonsmokers, 12 asymptomatic smokers, and 7 symptomatic subjects with chronic obstructive pulmonary disease (COPD) underwent two sets of back-to-back P_AO_2 imaging acquisitions in supine position with two opposite directions (top to bottom and bottom to top), followed by clinically standard pulmonary tests. The whole-lung mean, standard deviation (DP_AO_2) and vertical gradients of P_AO_2 along the slices were extracted, and the results were compared with clinically derived metrics. Statistical tests were performed to analyze the differences between cohorts.

Results—The anterior-posterior vertical gradients and DP_AO_2 effectively differentiated all three cohorts ($p<0.05$). The average vertical gradient P_AO_2 in healthy subjects was −1.03 ± 0.51 Torr/cm toward lower values in the posterior/dependent regions. The directional gradient was absent in smokers (0.36 ± 1.22 Torr/cm) and was in the opposite direction in COPD subjects (2.18 ± 1.54 Torr/cm). The vertical gradients correlated with Smoking History ($p=0.004$); BMI ($p=0.037$), PFT metrics (FEV_1, $p=0.025$; and %RV/TLC, $p=0.033$) and with distance walked in six minutes ($p=0.009$).

Discussion—Regional P_AO_2 data indicate that cigarette smoke induces physiological alterations that are not being detected by the most widely used physiologic tests.

Keywords

Alveolar Oxygen Tension; P_AO_2 Vertical Gradients

Corresponding Author: Rahim R. Rizi, University of Pennsylvania, Department of Radiology, 308 Stemmler Hall, 3450 Hamilton Walk, Philadelphia, PA, Tel: 215-573-0891, Fax: 215-746-8203, Rahim.rizi@uphs.upenn.edu.

INTRODUCTION

Non-invasive, regional assessment of lung function has the potential to markedly enhance early diagnosis and management of chronic obstructive pulmonary disease (COPD), to accelerate drug discovery and trials, and to provide fundamental insights into lung disease pathogenesis [1–4]. Accordingly, over the last decade, quantitative hyperpolarized gas MRI techniques have been developed to regionally investigate critical aspects of lung function and structure [5]. This approach has yielded several promising imaging parameters for regional evaluation of lung disease progression. These include regional measurements of alveolar oxygen tension (P_AO_2) [6–13], ventilation [14–17], perfusion [18,19], ventilation-to-perfusion ratio [20,21], and apparent diffusion coefficient ('ADC', a measure of lung microstructure). Although their refinement continues, particularly with respect to use with small animals, these imaging techniques have now been transferred successfully to humans. In this paper, we expand the potential of P_AO_2 imaging to detect variations in pulmonary function induced by smoking. Specifically, we demonstrate for the first time that it is possible to estimate the gravitational gradient in the alveolar oxygen tension in healthy supine subjects using a non-invasive imaging technique.

Hyperpolarized (HP) ^{3}He P_AO_2 imaging provides a quantitative and regional map of lung function−namely, the quality of local gas exchange and ventilation in parenchyma−that can serve as a powerful tool for the investigation of physiological changes in different lung diseases. This technique was introduced by Deninger *et. al* [6] and was subsequently modified [7,8] and optimized [9, 10] by many other investigators. In a previous study, we assessed the systematic variability of this technique in asymptomatic subjects [13]. Measurements of P_AO_2 changes with respect to disease severity have also been previously reported [11–13], and have shown that imaged P_AO_2 heterogeneity correlates with disease states and symptoms.

Here, we assess the ability of the P_AO_2 vertical gradient to detect changes in symptomatic and asymptomatic smokers. It was previously shown that the spatial variations in the lung provide sensitivity to early changes in some pulmonary diseases [11–13]. Other imaging and non-imaging studies have shown that the physiological gravity gradients observed in healthy subjects are altered in COPD patients and less so in smokers [22–29]. In this study, we evaluate the vertical P_AO_2 gradients observed in the anterior-posterior direction of the subject's lung to non-invasively estimate the gravitational gradients in the alveolar oxygen tension in healthy and unhealthy subjects. The estimated gradients are then compared to standard clinical pulmonary measurements and the sensitivity of this contrast to small, subclinical changes is assessed.

MATERIALS AND METHODS

Subject Groups

All human experiments were Health Insurance Portability and Accountability Act compliant. The study was performed under a protocol approved by the local Institutional Review Board, and all subjects signed an informed consent form prior to any test or experiment.

Twenty-seven human subjects, all 40–70 years of age, were grouped into three independent cohorts: healthy nonsmokers who had never smoked cigarettes; subjects with a smoking history of at least 20 pack-years and with a $FEV_1/FVC > 70\%$ and no clinical symptoms; and subjects diagnosed with COPD (Mild to Severe) or with both chronic cough and phlegm (Stage 0: based on ATS/ERS 2006 guidelines) as diagnosed by a pulmonary physician. The COPD 0 stage is no longer utilized in practice and has been removed from latest version of the Global Initiative for COPD criteria (ATS/ERS 2013 guideline). Nevertheless, the document does refer to these patients as abnormal but lacking sufficient evidence that they will necessarily progress to COPD.

Respiratory Clinical Tests

A standard clinical six minute walk (6MWT) was performed on all subjects at the beginning of each study. The distance traveled and maximum $SPO_2\%$ drop were recorded [30]. Immediately after the walk, subjects were asked to fill out a standard self-administered St. George's Respiratory Questionnaire (SGRQ), and the scores were calculated [31]. The questionnaire is divided into three subscales: symptoms (8 items), activity (16 items), and impacts (26 items). For each subscale in the questionnaire, scores range from zero (no impairment) to 100 (maximum impairment). An overall score is also calculated.

Prior to the imaging session (45 ± 15 minutes), all subjects underwent spirometry, plethysmography, a diffusing capacity test, and a six minute walk test in a hospital pulmonary function laboratory in accordance with ATS/ERS 2006 guidelines. Common parameters tested in this study included forced expiratory volume in 1 second (FEV_1), forced vital capacity (FVC), forced expiratory flow between 25% and 75% of the patient's exhaled volume ($FEF_{25–75\%}$), total lung capacity (TLC), residual volume (RV), diffusing capacity for carbon monoxide (DL_{CO}), the distance walked during a six minute walk test ($6MWT_D$), and the highest oxygen saturation drop recorded during the six minute walk test ($6MWT_{SPO2}$).

Imaging Technique

Depolarization of hyperpolarized gas in the lung is primarily caused by the RF pulses used in imaging and the dipole-dipole interaction of ^{3}He nuclei with the strong magnetic moments of the paramagnetic oxygen molecule. The longitudinal relaxation rate of HP ^{3}He depends linearly on the oxygen concentration [32]. In a series of back-to-back images with a flip angle of α, the ^{3}He spin density signal detectable in the n^{th} acquired image can be expressed as [9]:

$$S_n = S_0.[\cos(\alpha)]^{n.N_{PE}} \times \exp[-\mathrm{P_A O_2}.t_n/\xi] \quad (1)$$

where $\xi \approx 2.6$ [bar.sec] at body temperature, S_0 and S_n are the signal levels in the initial and n^{th} images, and t_n is the delay between the initial and n^{th} image. N_{PE} is the number of phase encoding excitations. In the case of a time-varying oxygen concentration, P_AO_2 in the above expression refers to the time-average between $t = 0$ and $t = t_n$.

P_AO_2 Scheme and Image Acquisition

For a successful decoupling of the oxygen-induced depolarization from that of the imaging pulses, a series of at least three back-to-back images is necessary, and the delays between successive images must differ. In this work, an interleaved multi-slice single-breath four-time-point acquisition was used for P_AO_2 imaging, covering the whole lung in coronal direction [9]. A gradient-echo imaging pulse sequence was used covering the lung with N_S = 12 slices (slice thickness; ST = 13 mm) and an inter-slice gap of 20% ST, with the field of view = 40×30 cm^2, matrix size = 48×36, $\alpha_{nominal}$ = 5°, and T_R/T_E = 6.8/3.1 ms. For each slice, two interleaved sets of back-to-back images with no time gap (slice imaging time = $N_{PE} \times T_R = 36 \times 6.8 = 0.25$ sec) were repeated for the whole lung. This scheme results in four time points in an AABBCC…LLAABBCC…LL manner with a time interval vector for slice s of $\boldsymbol{t_{n,s}} = 2N_{PE}T_R \times [s\text{-}1\ s\text{-}½\ N_S + s\text{-}1\ N_S + s\text{-}½]$ seconds. Analysis yields a P_AO_2 map for each slice with a voxel size of 8.3×8.3×15.6 mm^3 in a 12-second breath-hold.

A whole-body 1.5-T MRI scanner (MAGNETOM Sonata, Siemens Medical Solutions, Malvern, PA) generated the ^{3}He images using a chest coil with an 8-channel receive and a separate, saddle-shaped transmit coil (Stark Contrast, Erlangen, Germany) tuned to 48.48 MHz ^{3}He resonance frequencies.

HP ^{3}He Production

Imaging gas (^{3}He:N_2 = 99.19:0.81, Linde, Branchburg, NJ) was hyperpolarized using a commercial prototype polarizer (IGI 9600.He, GE Healthcare, Durham, NC) through spin-exchange collisions with optically pumped rubidium atoms. Polarization levels of 25–35% were achieved after 15 hours of optical pumping.

Human Experiments

Two Tedlar bags, one containing a mixture of the hyperpolarized gas with pure N_2 and the other containing O_2 gas, were transferred to the MRI scanner, where they were connected to a three-way pneumatic valve. The total inhaled gas volume equaled 12% of the subject's TLC, and FiO_2 was kept at approximately 21%. Subsequent to the actuation of a pneumatic valve, the subject was instructed to inhale the full contents of both bags simultaneously and then to begin a 12 second breath-hold. We did not perform an independent measurement to confirm the fraction of the gas inhaled by the subject; however enough practice was performed to make sure the contents of both bags are inhaled. Immediately after the breath-hold, the subject exhaled back into the Tedlar bags, and the exhaled gas was collected and analyzed with a gas analyzer (CWE Inc., GEMINI Respiratory Gas Analyzer, Ardmore, PA) for the fraction of exhaled oxygen and carbon dioxide (mixed-expired PEO_2 and $PECO_2$). The subjects' vital signs were monitored at 5-minute intervals throughout the imaging session under the supervision of a technician.

Two sets of P_AO_2 imaging were performed on each subject in the supine position approximately 5 minutes apart. In the first set, the multi-slice acquisition was performed from the anterior slice (A) to the posterior slice (P); in the second set, the direction of image acquisition was changed (P to A).

Image Analysis

Custom software was developed using MATLAB (MathWorks, Inc., Natick, MA) for image analysis. Prior to the analysis, the acquired signal was bias-corrected for the background noise according to $\hat{S}=\sqrt{S^2-\sigma^2}$, where $\hat{S}=\overline{B}\sqrt{2/\pi}$ and $\bar{B}$ is the average background noise. For lung segmentation, Contrast Limited Adaptive Histogram Equalization (CLAHE) was used to improve the contrast in the images [33] followed by Ostu's method to automatically threshold [34] each of the four-time-point raw ^{3}He spin density images to mask the background noise. The lung was then segmented based on all the four-time-point ^{3}He images for each slice, where voxels were included for at least 2 of the four masked images.

Two separate sets of slice-by-slice P_AO_2 images were computed using a least-squares fit of a model (Equation 1) of RF-corrected O_2-induced relaxation: i) to each voxel's signal intensity drop in the image series, and ii) to each slice's sum of all voxels' signal drop in the four time-point series (slice P_AO_2). Across all twelve slices, the mean (MP_AO_2) and standard deviation (DP_AO_2) of all voxels' P_AO_2 were calculated from a Gaussian fit to the whole-lung distribution histogram generated from i) and a slice P_AO_2 value (SP_AO_2) from ii) for each slice. The latter fit has higher accuracy since it is estimated from the sum of all the signals in each slice (i.e., much higher SNR). This analysis was separately performed for A→P and P→A acquisitions.

Complete acquisition of the images for each slice (four time-points) takes about 6 seconds, and assuming a constant rate of oxygen uptake during this time, the resulting map for each slice corresponds to the P_AO_2 midway through the imaging sequence for that specific slice; that is, for slice s in acquisition order out of a total of N_S,

$$P_AO_2=P_AO_2(0)-V\dot{O}_2N_{PE}T_R(N_S+2s-{}^3\!/_2) \quad (2)$$

where, $P_AO_2(0)$ is the true oxygen concentration at the beginning of the imaging sequence, and $V\dot{O}_2$ is the constant rate of oxygen uptake.

Vertical Gradients

Figure 1 illustrates the strategy we used to calculate the corrected vertical gradients from the two opposite directions of MRI acquisition (A→P and P→A). The anterior-posterior P_AO_2 gradient along the slices in this imaging scheme originates from two distinct mechanisms: 1) the different imaging time for each slice, and 2) the known physiological gravity effects on both ventilation and perfusion [22,35–38]. In the multislice imaging scheme used in this study, it takes approximately 12 seconds for the imaging sequence to cover the whole lung. During this time, the presence of oxygen uptake results in a lower oxygen level in the slices that are imaged later. As a result, the two opposite imaging acquisitions produce different P_AO_2 values for the identical slices. To correct for this effect and thereby estimate the true vertical gradient in the lung, we averaged the P_AO_2 acquired from the two opposite imaging

directions for identical slices. Note that the image acquisition order is opposite for the two directions, i.e.,

$$s_{P\to A}=N_S+1-s_{A\to P} \quad (3)$$

Thus, if the two measured P_AO_2 values are averaged,

$$\overline{P_AO_2}=\frac{1}{2}[(P_AO_{2_{A\to P}}+P_AO_{2_{P\to A}}]=P_AO_2(0)-V\dot{O}_2N_{PE}T_R(2N_S-\frac{1}{2}) \quad (4)$$

and the dependence on slice acquisition order is eliminated.

The global P_AO_2 (SP_AO_2; computed from the sums of signals in each slice) for the identical slices of A→P and P→A acquisition were averaged to cancel the effect of oxygen uptake during the breath-hold. The pure spatial gradient was then estimated by fitting a line to $SP_AO_2(z)$ as a function of slice position *z*, weighted by $1/\sqrt{SEM^2_{A\to P}+SEM^2_{P\to A}}$, where standard errors of means (*SEM*) for each slice were estimated as $\sigma/\sqrt{n}$; σ and n are the standard deviation of P_AO_2 (DP_AO_2) and the number of valid voxels in the given slice, respectively. The most anterior and most posterior slices were excluded in this procedure due to the greater inhomogeneity of coil profiles close to the surface of the coils as well as the partial volume effects resulting from sub-voxel motions of lung boundaries. Generally, the fit quality of P_AO_2 in the first and last slices is noticeably lower. After these operations, and in the absence of confounding effects to be discussed later, the resulting slope of $\overline{P_AO_2}(z)$ represents the pure physiologic gradient.

Global alveolar partial pressure of oxygen

To elucidate the validity of our oxygen measurements, the expected $\widehat{P_AO_2}$ was estimated from the mixed-expired gas analysis. Global alveolar oxygen tension ($\widehat{P_AO_2}$) was roughly approximated assuming a two-compartment model in the Tedlar bag containing the mixed-expired gas: 1) a dead space compartment and 2) an alveolar compartment. Dead space volume (V_d) was estimated based on the subjects' weight [39]. The total subject's expired gas volume assumed to be equal to the Tedlar bag volume. Based on subjects' TLC, two different bag sizes were used: 500 ml for TLC < 5 liters and 1000 ml for TLC >5 liters. The alveolar compartment's oxygen fraction was derived from:

$$\widehat{P_AO_2}=\frac{P_{\bar{E}}O_2\times V_{Bag}-P_IO_2\times V_d}{V_{Bag}-V_d}$$

This rough estimation of $\widehat{P_AO_2}$ was regressed against the HP imaged P_AO_2 measured from a least-squares fit of a model (Equation 1) to the whole lung's sum of all voxels' signal drop in the four time-point series (global P_AO_2). This regression model serves as a measure of

departure of the expected $\widehat{P_A O_2}$ from the measured HP imaged $P_A O_2$. We interpret the intercept of this regression to indicate bias in the oxygen measurements.

Statistical Analysis

All statistical analysis was performed using the R software [40]. R is an open-source project that is distributed under the GNU General Public License (Copyright 2007 Free Software Foundation, Inc.). Univariate *Pearson* correlations were used to analyze the relationship between MRI measures of respiratory function and important non-imaging measurements.

To investigate whether multiple levels of combined measured variables are statistically different among the cohorts, multivariate analysis of variance was performed. For each variable, ANOVA models were analyzed separately to compare all the possible paired combinations of the variable cohorts; this was followed by post hoc tests only for the variables that were significant. For post hoc analysis, the Tukey HSD test was used, which provides the mean difference between each cohort and a *p* value to indicate whether two cohorts are significantly different. A 95% confidence interval was also computed for each pair. The Tukey method is fundamentally a *t*-test that corrects for experiment-wise error rate (type I), and it is thus more appropriate than a normal *t*-test for multivariate comparisons in multiple cohorts. An alpha level of 0.05 was considered significant in all analyses.

RESULTS

Non-imaging clinical tests (Demographics, PFT, 6MWT and SGRQ)

The 27 subjects enrolled in this study were classified into three cohorts: eight healthy subjects with no history of smoking (HN: 4M, 50±7 years old), twelve asymptomatic smokers (AS: 7M, 48±5 years old, 29±5 pack-years), and seven symptomatic smokers with clinical symptoms (symptomatic smokers: 4M, 58±9 years old, 41±8 pack-years). The symptomatic smokers group contained three subjects diagnosed with moderate COPD (Stage II: 2M, 58±14 years old, 43±11 pack-years), one with severe COPD (Stage III: M, 62 years old, 35 pack-years) and three subjects exhibiting chronic cough and phlegm (Stage 0: 1M, 56±14 years old, 41±8 pack-years, SGRQ overall score 31±17%). Figure 2 demonstrates the boxplots of the subjects' demographics, a subset of pulmonary function test parameters, SGRQ scores, and 6MWT distance. Table 1 summarizes the analysis of variance results for the three cohorts (for more details, see online supplementary table). The three cohorts (HN, AS, and SS) were not significantly different with respect to body mass index (BMI) and TLC. Aside from the obvious smoking history, the healthy nonsmokers and asymptomatic smokers did not differ in age, FEV_1, FEV_1/FVC, DL_{CO}, FEV_1% pred., $6MWT_{SPO2}$, and SGRQ overall score. Symptomatic smokers smoked significantly more than asymptomatic subjects and were older and had significantly worse FEV_1, FEV_1/FVC, DL_{CO}, FEV1% pred., RV/TLC % pred., and SGRQ overall. While the distance symptomatic smokers subjects walked in six minutes ($6MWT_D$) is not different from that of healthy nonsmokers and asymptomatic smokers, the maximum drop in oxygen saturation level ($6MWT_{SPO2}$) during the walk of symptomatic subjects was significantly more than that of healthy nonsmokers.

^{3}He MRI alveolar oxygen tension

Figure 3 shows the ^{3}He MRI P_AO_2 maps (oxygen tension) for a healthy and a COPD subject. This figure qualitatively shows the variation in spin density and oxygen tension across the lung. The heterogeneity of the maps is increased in the COPD subject compared to the healthy—a quality that was also generally observed in the symptomatic smoker subjects not shown. The whole-lung averages and standard deviations ($MP_AO_2 \pm DP_AO_2$) were extracted from a Gaussian fit to the whole-lung distribution. Table 2 lists the whole-lung averages and standard deviations as well as the results of collected end-tidal gas analysis (exhaled partial pressure of carbon dioxide) for A→P and P→A in all individual subjects. The average MP_AO_2 (all voxel's P_AO_2) in all subjects for the two directions of acquisition does not differ (*H1*: MP_AO_2 (A→P) ≠ MP_AO_2 (P→A); $p = 0.98$), and the global average for all the subjects and all the experiments (97.03 Torr) is consistent with the prediction of the alveolar gas equation ($P_AO_2 = F_IO_2(P_{ATM} - pH_2O) - P_aCO_2/RQ = 99.7$ Torr). It should be mentioned that the imaged P_AO_2 is less than $P_AO_2(0)$ due to oxygen uptake during the breath-hold. The results of analysis of variance for both directions of P_AO_2 separately among the three cohorts are listed in Table 3. The MP_AO_2 (whole-lung average) measurements are not significantly different among the cohorts. However, the DP_AO_2 (whole-lung standard deviation)—a measure of heterogeneity—significantly increases from healthy subjects to asymptomatic smokers subjects (in the case of anterior to posterior acquisition) and from the asymptomatic smokers cohort to the symptomatic smokers cohort (see Table 3 for the statistic significances).

Figure 4 shows the association between the estimated $\widehat{P_AO_2}$ (derived from the mixed-expired PEO_2) and imaged global HP P_AO_2 for all of the studies. Regressing the estimated $\widehat{P_AO_2}$ on the global imaged HP P_AO_2 gave a slope of 0.90 (SE: 0.113; $p < 0.001$). The constant term was found to be 10.5 Torr.

Slopes of P_AO_2 gradients along the slices

Figure 5 represents the imaged whole-slice P_AO_2 as a function of the distance from the most dependent/posterior region of the subject's lung. Each column shows a group-averaged observation for all of the subjects in that group (HN, AS, and SS). This figure shows the average of the two acquisition directions ($\overline{P_AO_2}$), which was computed to correct for bias related to the uptake of oxygen and the order of acquisition (refer to the Methods section). The observed slope of the linear fit is therefore more closely related to the true vertical gradient of P_AO_2.

Table 4 shows the derived gradient slopes for both acquisitions ($S_{A\to P}$ and $S_{P\to A}$) and the resulting corrected gradient computed from the two opposing directions $\left(\frac{A\to P + P\to A}{2}\right)$, for all the subjects from the three cohorts. In healthy nonsmokers subjects, all the observed P_AO_2 gradients in both imaging directions (A→P and P→A) trend toward higher values when moving from the posterior to the anterior slices with one exception in which the gradient was in the opposite direction in the P→A acquisition (HN-05). This results in a corrected vertical gradient slope (−1.03 ± 0.51 Torr/s) in the same direction as the A→P and P→A cases (higher in anterior slices). In the case of the asymptomatic smoker subjects, the

same observation is true for the A→P acquisitions in 9 out of the 12 cases; the anterior slices still have higher values than the middle and posterior slices, although the slope changed direction in all but one of the asymptomatic smoker subjects (AS-04) for the P→A acquisition. This change in gradient direction leads to an insignificant corrected (averaged) vertical gradient for the whole asymptomatic smoker cohort (vertical gradient = 0.36 ±1.22). The large deviations between the A→P and P→A slopes in asymptomatic smoker subjects resulted in a high standard deviation in this group. In nearly all of the symptomatic smoker subjects, the slopes are completely opposite to those of the healthy nonsmoker group—i.e., the posterior slices show higher values than the middle and anterior slices in both A→P and P→A directions. As a result, the vertical gradient is significantly positive (vertical gradient = 2.18 ±1.54).

Vertical gradients differences among cohorts

Table 5 shows a summary of the differences among the cohorts based on the observed gradients in A→P and P→A imaging directions and the resulting vertical gradients. The symptomatic smoker subjects can be effectively distinguished from the healthy nonsmoker and asymptomatic smoker cohorts based on each of the three sets of gradient slopes ($S_{A\rightarrow P}$, $S_{P\rightarrow A}$ and vertical gradient). The $S_{A\rightarrow P}$ can also differentiate the symptomatic from asymptomatic smokers. While none of the individual gradient slopes of $S_{A\rightarrow P}$ or $S_{P\rightarrow A}$ are able to distinguish the asymptomatic smokers from nonsmokers ($p > 0.05$), the computed pure vertical gradient slopes from the two acquisition schemes differentiate all three cohorts from each other.

Correlations between gradients and non-imaging parameters

Figure 6 offers a graphical view of associations between the measured corrected vertical gradients and the clinical tests. Smoking history and BMI directly correlate with vertical gradient for the subjects in this study. There is no association between FEV_1/FVC and the gradients, but FEV_1 negatively correlate with the gradients. DLCO shows a weak but non-significant negative association with vertical gradient ($p = 0.055$). A significant correlation exists between vertical gradient and RV/TLC, which is a measure of air trapping. Finally, subjects' walking distance in six minutes inversely correlates with vertical gradient, while SGRQ overall score directly correlates with vertical gradient (not shown).

DISCUSSION

In this study, we expanded the application of P_AO_2 imaging to detect physiological variations in pulmonary function induced by smoking. We were able to estimate the gravitational gradient in the alveolar oxygen tension using a non-invasive imaging technique in healthy subjects in supine position. We subsequently compared the P_AO_2 vertical gradients of healthy non-smokers, asymptomatic smokers, and symptomatic smokers. This study demonstrated that the imaging derived P_AO_2 vertical gradients are capable of differentiating between the lung function of non-smokers, asymptomatic smokers, and COPD patients.

We have previously shown that P_AO_2 maps are sensitive to small changes in lung function; specifically, the heterogeneity of P_AO_2 maps was significantly larger in diseased lung [9,13]. In addition, this work added to the contrasts that can be derived via hyperpolarized gas MRI by demonstrating that P_AO_2 vertical gradients differed significantly among the three groups. In all the healthy subjects studied, P_AO_2 decreased from anterior to posterior regions regardless of which direction the multi-slice MRI acquisitions were performed (anterior to posterior and vice versa). In asymptomatic smokers, 75% of the cohort exhibited higher P_AO_2 in anterior slices than posterior when imaging was performed in the A→P direction, although the average slope was reduced. This trend reversed when we imaged P→A. After averaging the P_AO_2 of each slice to cancel out the effect of oxygen uptake, the apparent vertical gradient for the asymptomatic smoker cohort was lost, an effect also observed in other recent studies [23,24]. Finally, in the case of the symptomatic cohort (with two exceptions), the trend observed in healthy subjects was completely reversed in both A→P and P→A acquisitions. COPD subjects actually showed larger P_AO_2 values in dependent regions.

While both the elevated heterogeneity of oxygen tension and the loss of vertical gradients separated the three cohorts with a highly significant statistical power, the vast majority of the clinical tests (PFT, 6MWT and SGRQ) — although able to differentiate the COPD group — did not differentiate between healthy non-smokers and asymptomatic smokers. The latter set of pulmonary tests only provides a global knowledge of lung function, and it is thus incapable of detecting early, small, localized changes associated with smoking. These changes may be related to early disease, although the present study does not support that conclusion.

In addition to distinguishing between the three cohorts, the P_AO_2 gradients meaningfully associated with a number of the well-established clinical tests, suggesting that the gradients are reflective of various smoking-induced functional changes. The weak but significant relationship between vertical P_AO_2 gradients and spirometric indices was confirmed by the gradients' correlation with FEV_1 and $FEF_{25–75\%}$, both sensitive measures of obstructive pathologies. The gradients exhibited a weak (nonsignificant) correlation with FEV_1 percent predicted ($p = 0.052$), which is an important criterion for GOLD diagnosis of COPD patients. Increased RV/TLC, as a measure of both pulmonary obstruction and restriction—also relate to "air trapping" in the lung—had the strongest association with the vertical gradient of P_AO_2. The observed vertical gradient also showed a weak (nonsignificant) correlation with DL_{CO}. No correlation was observed with FEV_1/FVC, the most common spirometry parameter in PFTs. A correlation between the imaged alveolar oxygen tension and the rough estimation of $\widehat{P_AO_2}$ based on the mixed-expired gas analysis ($r = 0.75$, $p < 0.001$) was also demonstrated. The observed offset (~10 Torr) in these measurements is likely the result of error induced in calculation of $\widehat{P_AO_2}$ due to the assumptions we made in this estimation: dead space was estimated based on weight, FiO_2 was assumed to be 21% for all the subjects and the total exhaled gas volume was assumed to be the Tedlar bag's volume. It should also be noted that the imaged P_AO_2 and estimated $\widehat{P_AO_2}$ do not belong to the same

time point; the estimated $\widehat{P_AO_2}$ belongs to the end of the 12-second breath-hold, while imaged P_AO_2 shows the oxygen tension midway through the imaging sequence.

The gravity gradient is admittedly a very complicated concept [35–38], and its interpretation still poses a challenge in the field of pulmonary physiology [37]. Nonetheless, in the case of healthy nonsmokers, our range of corrected vertical gradients is in accordance with West's [35] findings, which suggests that the P_AO_2 gradients are real observed physiology. The average of the estimated vertical gradient in supine healthy normal subjects (-1.03 ± 0.51 Torr/cm) was slightly less than what West [35] reported in upright human subjects (−1.5 Torr/cm, obtained from the slope of a linear fit to his reported P_AO_2 in different heights of the lung). This lower average in supine position can be explained by previous studies, which demonstrated that the effect of gravity on pulmonary function is dependent on body posture and is larger when upright [38].

In the case of smokers and COPD subjects, research is still in progress to explain the loss of the vertical gradient. Consequently, it is not yet entirely clear if and how a decline in P_AO_2 gradient is reflective of physiological alterations caused by smoking. This decline could be related to a whole host of smoking-induced changes in the properties of the lung. Michaels et al., [41], for example, found that cigarette smoke may damage the elastic properties [42] of the lungs. Moreover, ventilation and ventilation-to-perfusion ratio decrease in the basal lung regions of subjects with chronic bronchitis, while patients with early emphysema exhibit a relative reduction in ventilation and perfusion in the upper zones [29, 43–45]. Melo *et al.*, [24] studied perfusion and ventilation in COPD subjects using ^{13}N PET. They observed an anterior-posterior gradient (larger in the dependent region) in healthy subjects, but not in COPD. They also reported greater heterogeneity of perfusion and ventilation–perfusion ratio in COPD patients. Several other investigators have shown that pulmonary hypertension and vascular/airway remodeling can change the regional distribution of ventilation and perfusion [23,46].

It is also possible that the observed vertical gradient contrast between healthy and diseased subjects originates from abnormal gas redistribution in the diseased lung during the end-inspiratory 12-second breath-hold required for imaging. The P_AO_2 imaging technique is highly dependent on gas dynamics, so it is possible that artifacts arising from gas flow during the breath-hold could be in some extent responsible for the altered gradients. Marshall *et al* and Hamedani *et al* reported the limitations of the P_AO_2 technique in severely diseased subjects, which results in non-physiological P_AO_2 values in regions where significant gas flow is present during the breath-hold [9,13, 47,48]. The gas motion during the breath-hold is minimal in healthy subjects, or is at least not made evident by gas MRI. However, in the case of symptomatic subjects, the probable gas redistribution during breath-hold can skew the results in diseased regions. In regions with high diffusion and in presence of gas flow, the change in the location of gas signal can mimic the effect of oxygen. In a limiting case, when gas first reaches a voxel after the first image (due to slow filling), the fit to P_AO_2 equation results in very low or even negative values—since flow is not explicitly included in the modeled signal dynamics, increasing signal is interpreted as the 'depolarization' arising from a negative oxygen. Using the sum of entire voxels' signal for computation of slice P_AO_2 instead of calculating the average of voxel-by-voxel P_AO_2

computations cancels the artifacts originated from gas transfer between voxels in each slice. Nevertheless, the gas flow is still present between the slices (~15 mm), and this can skew the results in diseased regions. The presence of these artifacts in symptomatic subjects should therefore cause us to take care in attributing alterations in the P_AO_2 gradient entirely to physiological phenomena, although the ability of the technique to highlight subclinical alterations is useful regardless of the origin of the contrast.

CONCLUSION

The suite of imaged P_AO_2 parameters may provide an extremely useful diagnostic tool for the detection of smoking-related alterations in lung function. Both DP_AO_2 and the newly developed P_AO_2 vertical gradient successfully differentiated between healthy non-smoker, asymptomatic smoker, and COPD subjects, a distinguishing power that was not observed in conventional clinical measurements of pulmonary function. The weak correlations that were observed between the P_AO_2 parameters and many of the clinical tests suggest that the P_AO_2 vertical gradients measure a physiologic abnormality not appreciated in routine pulmonary function tests. This combination of results indicates that cigarette smoke induces alterations in the lung that are not being captured by the most widely used clinical tests. Further investigation of P_AO_2 imaging techniques and lung physiology will help to elucidate the origin of these previously hidden changes.

Supplementary Material

Refer to Web version on PubMed Central for supplementary material.

Acknowledgments

Grant Number: NIH R01-HL089064

References

1. Washko GR, Lynch DA, Matsuoka S, Ross JC, Umeoka S, Diaz A, Sciurba FC, Hunninghake GM, Estépar RS, Silverman EK, Rosas IO, Hatabu H. Identification of early interstitial lung disease in smokers from the COPDGene Study. Academic Radiology. 2010; 17(1):48–53. [PubMed: 19781963]
2. Schroeder JD, McKenzie AS, Zach JA, Wilson CG, Curran-Everett D, Stinson DS, Newell JD Jr, Lynch DA. Relationships between airflow obstruction and quantitative CT measurements of emphysema, air trapping, and airways in subjects with and without chronic obstructive pulmonary disease. American Journal of Roentgenology. 2013; 201(3):W460–W470. [PubMed: 23971478]
3. Hopkins SR, Prisk GK. Lung perfusion measured using magnetic resonance imaging: New tools for physiological insights into the pulmonary circulation. Journal of Magnetic Resonance Imaging. 2010; 32(6):1287–1301. [PubMed: 21105135]
4. van Beek EJ, Wild JM, Kauczor HU, Schreiber W, Mugler JP 3rd, de Lange EE. Functional MRI of the lung using hyperpolarized 3-helium gas. Journal of Magnetic Resonance Imaging. 2004; 20(4): 540–554. [PubMed: 15390146]
5. Fain S, Schiebler ML, McCormack DG, Parraga G. Imaging of lung function using hyperpolarized helium-3 magnetic resonance imaging: Review of current and emerging translational methods and applications. Journal of Magnetic Resonance Imaging. 2010; 32(6):1398–1408. [PubMed: 21105144]

6. Deninger AJ, Eberle B, Bermuth J, Escat B, Markstaller K, Schmiedeskamp J, Schreiber WG, Surkau R, Otten E, Kauczor HU. Assessment of a single-acquisition imaging sequence for oxygen-sensitive 3He-MRI. Magnetic Resonance in Medicine. 2002; 47(1):105–114. [PubMed: 11754449]
7. Wild JM, Fichele S, Woodhouse N, Paley MN, Kasuboski L, van Beek EJ. 3D volume-localized pO2 measurement in the human lung with 3He MRI. Magnetic Resonance in Medicine. 2005; 53(5):1055–1064. [PubMed: 15844148]
8. Miller GW, Mugler JP 3rd, Altes TA, Cai J, Mata JF, de Lange EE, Tobias WA, Cates GD, Brookeman JR. A short-breath-hold technique for lung pO2 mapping with 3He MRI. Magnetic Resonance in Medicine. 2010; 63(1):127–136. [PubMed: 19918891]
9. Hamedani H, Kadlecek SJ, Emami K, Kuzma NN, Xu Y, Xin Y, Mongkolwisetwara P, Rajaei J, Barulic A, Wilson Miller G, Rossman M, Ishii M, Rizi RR. A multislice single breath-hold scheme for imaging alveolar oxygen tension in humans. Magnetic Resonance in Medicine. 2010; 67(5): 1332–1345. [PubMed: 22190347]
10. Yu J, Ishii M, Law M, Woodburn JM, Emami K, Kadlecek S, Vahdat V, Guyer RA, Rizi RR. Optimization of scan parameters in pulmonary partial pressure oxygen measurement by hyperpolarized 3He MRI. Magnetic Resonance in Medicine. 2008; 59(1):124–131. [PubMed: 18050348]
11. Deninger AJ, Eberle B, Ebert M, Grossmann T, Hanisch G, Heil W, Kauczor HU, Markstaller K, Otten E, Schreiber W, Surkau R, Weiler N. (3)he-MRI-based measurements of intrapulmonary pO2 and its time course during apnea in healthy volunteers: first results, reproducibility, and technical limitations. NMR in Biomedicine. 2000; 13(4):194–201. [PubMed: 10867696]
12. Gast KK, Biedermann A, Herweling A, Schreiber WG, Schmiedeskamp J, Mayer E, Heussel CP, Markstaller K, Kauczor HU, Eberle B. Oxygen-sensitive 3He-MRI in bronchiolitis obliterans after lung transplantation. European Radiology. 2008; 18(3):530–537. [PubMed: 17926041]
13. Hamedani H, Kadlecek SJ, Ishii M, Emami K, Kuzma NN, Xin Y, Rossman M, Rizi RR. A variability study of regional alveolar oxygen tension measurement in humans using hyperpolarized 3He MRI. Magnetic Resonance in Medicine. 2013; 70(6):1557–1566. [PubMed: 23382040]
14. Emami K, Xu Y, Hamedani H, Xin Y, Profka H, Rajaei J, Kadlecek S, Ishii M, Rizi RR. Multislice fractional ventilation imaging in large animals with hyperpolarized gas MRI. NMR in Biomedicine. 2012; 25(9):1015–1025. [PubMed: 22290603]
15. Emami K, Xu Y, Hamedani H, Profka H, Kadlecek S, Xin Y, Ishii M, Rizi RR. Accelerated fractional ventilation imaging with hyperpolarized Gas MRI. Magnetic Resonance in Medicine. 2013; 70(5):1353–1359. [PubMed: 23400938]
16. Mathew L, Kirby M, Etemad-Rezai R, Wheatley A, McCormack DG, Parraga G. Hyperpolarized 3He magnetic resonance imaging: Preliminary evaluation of phenotyping potential in chronic obstructive pulmonary disease. European Journal of Radiology. 2011; 79(1):140–146. [PubMed: 19932577]
17. Kirby, M. Thesis. 2013. Pulmonary Structure and Function in Chronic Obstructive Pulmonary Disease Evaluated using Hyperpolarized Noble Gas Magnetic Resonance Imaging. http://ir.lib.uwo.ca/cgi/viewcontent.cgi-article=2492&context=etd
18. Qing K, Ruppert K, Jiang Y, Mata JF, Miller GW, Shim YM, Wang C, Ruset IC, Hersman FW, Altes TA, Mugler JP 3rd. Regional mapping of gas uptake by blood and tissue in the human lung using hyperpolarized xenon-129 MRI. Magnetic Resonance Imaging. 2014; 39(2):346–359.
19. Kaushik SS, Freeman MS, Cleveland ZI, Davies J, Stiles J, Virgincar RS, Robertson SH, He M, Kelly KT, Foster WM, McAdams HP, Driehuys B. Probing the regional distribution of pulmonary gas exchange through single-breath gas-and dissolved-phase 129Xe MR imaging. Journal of Applied Physiology. 2013; 115(6):850–860. [PubMed: 23845983]
20. Rizi RR, Baumgardner JE, Ishii M, Spector ZZ, Edvinsson JM, Jalali A, Yu J, Itkin M, Lipson DA, Gefter W. Determination of regional VA/Q by hyperpolarized 3He MRI. Magnetic resonance in medicine. 2004; 52(1):65–72. [PubMed: 15236368]
21. Mugler JP 3rd, Altes TA, Ruset IC, Dregely IM, Mata JF, Miller GW, Ketel S, Ketel J, Hersman FW, Ruppert K. Simultaneous magnetic resonance imaging of ventilation distribution and gas uptake in the human lung using hyperpolarized xenon-129. Proceedings of the National Academy of Sciences. 2010; 107(50):21707–21712.

22. Glenny RW, Robertson HT. Spatial distribution of ventilation and perfusion: mechanisms and regulation. Comprehensive Physiology. 2011; 1(1):375–395. [PubMed: 23737178]
23. Lau EM, Bailey DL, Bailey EA, Torzillo PJ, Roach PJ, Schembri GP, Corte TJ, Celermajer DS. Pulmonary hypertension leads to a loss of gravity dependent redistribution of regional lung perfusion: a SPECT/CT study. Heart. 2014; 100(1):47–53. [PubMed: 24186566]
24. Vidal Melo MF, Winkler T, Harris RS, Musch G, Greene RE, Venegas JG. Spatial heterogeneity of lung perfusion assessed with (13)N PET as a vascular biomarker in chronic obstructive pulmonary disease. J Nuclear Medicine. 2010; 51(1):57–65.
25. Sá RC, Cronin MV, Henderson AC, Holverda S, Theilmann RJ, Arai TJ, Dubowitz DJ, Hopkins SR, Buxton RB, Prisk GK. Vertical distribution of specific ventilation in normal supine humans measured by oxygen-enhanced proton MRI. Journal of Applied Physiology. 2010; 109(6):1950–1959. [PubMed: 20930129]
26. Burrowes KS, Tawhai MH. Computational predictions of pulmonary blood flow gradients: gravity versus structure. Respiratory Physiology & Neurobiology. 2006; 154(3):515–523. [PubMed: 16386472]
27. Burrowes KS, Hunter PJ, Tawhai MH. Investigation of the Relative Effects of Vascular Branching Structure and Gravity on Pulmonary Arterial Blood Flow Heterogeneity via an Image-based Computational Model. J Academic Radiology. 2005; 12(11):1464–1474.
28. Fichele S, Woodhouse N, Swift AJ, Said Z, Paley MN, Kasuboski L, Mills GH, van Beek EJ, Wild JM. MRI of helium-3 gas in healthy lungs: Posture related variations of alveolar size. Magnetic Resonance Imaging. 2004; 20(2):331–335.
29. Evans A, McCormack D, Ouriadov A, Etemad-Rezai R, Santyr G, Parraga G. Anatomical distribution of 3He apparent diffusion coefficients in severe chronic obstructive pulmonary disease. Journal of Magnetic Resonance Imaging. 2007; 26(6):1537–1547. [PubMed: 17968961]
30. Enright PL. The six-minute walk test. Respiratory Care. 2003; 48:783–785. [PubMed: 12890299]
31. Jones PW, Quirk FH, Baveystock CM. The St George's respiratory questionnaire. Respiratory Medicine. 1991; 85:25–31. [PubMed: 1759018]
32. Saam B, Happer W, Middleton H. Nuclear relaxation of 3He in the presence of O2. Physical Review A. 1995; 52(1):862–865.
33. Pizer SM, Amburn EP, Austin JD, Cromartie R, Geselowitz A, Greer T, Romeny BH, Zimmerman JB, Zuiderveld K. Adaptive histogram equalization and its variations. Computer Vision, Graphics, and Image Processing. 1987; 39(3):355–368.
34. Otsu N. A threshold selection method from gray-level histograms. Automatica. 1975; 11(285–296):23–27.
35. West JB. Regional differences in gas exchange in the lung of erect man. Applied Physiology. 1963; 17:893–898.
36. West JB, Dollery CT. Distribution of blood flow and ventilation-perfusion ratio in the lung, measured with radioactive carbon dioxide. Applied Physiology. 1960; 15:405–410.
37. Glenny RW, Robertson HT. Spatial distribution of ventilation and perfusion: mechanisms and regulation. Comprehensive Physiology. 2011; 1(1):375–395. [PubMed: 23737178]
38. Kaneko K, Milic-Emili J, Dolovich MB, Dawson A, Bates DV. Regional distribution of ventilation and perfusion as a function of body position. Applied Physiology. 1966; 21:767–777.
39. Hart MC, Orzalesi MM, Cook CD. Relation between anatomic respiratory dead space and body size and lung volume. Applied Physiology. . 1963; 18(3):519–522.
40. R Development Core Team: R: A language and environment for statistical computing. R Foundation for Statistical Computing. Vienna, Austria: ISBN; 3-900051-07-0. Available at: http://www.r-project.org. [Accessed October 9, 2009]
41. Michaels R, Sigurdson M, Thurlbeck S, Cherniack R. Elastic recoil of the lung in cigarette smokers: the effect of nebulized bronchodilator and cessation of smoking. Am Rev Respir Dis. 1979; 119(5):707–16. [PubMed: 453696]
42. Hopkins SR, Henderson AC, Levin DL, Yamada K, Arai T, Buxton RB, Prisk GK. Vertical gradients in regional lung density and perfusion in the supine human lung: the Slinky effect. Applied Physiology. 2007; 103:240–248.

43. Buist AS, Vollmer WM, Johnson LR, McCamant LE. Does the single-breath N2 test identify the smoker who will develop chronic airflow limitation? American Review of Respiratory Disease. 1988; 137:293–301. [PubMed: 3341624]

44. Anthonisen NR, Bass H, Oriol A, Place RE, Bates DV. Regional lung function in patients with chronic bronchitis. Clinical Science. 1968; 35:495–511. [PubMed: 5705805]

45. Gaziano D, Seaton A, Ogilvie C. Regional lung function in patients with obstructive lung diseases. British Medical. 1970; 2(5705):330–333.

46. Santos S, Peinado VI, Ramírez J, Melgosa T, Roca J, Rodriguez-Roisin R, Barberà JA. Characterization of pulmonary vascular remodelling in smokers and patients with mild COPD. European Respiratory. 2002; 19(4):632–638.

47. Marshall H, Parra-Robles J, Deppe MH, Lipson DA, Lawson R, Wild JM. 3He pO2 mapping is limited by delayed-ventilation and diffusion in chronic obstructive pulmonary disease. Magnetic Resonance in Medicine. 2013

48. Marshall H, Deppe MH, Parra-Robles J, Hillis S, Billings CG, Rajaram S, Swift A, Miller SR, Watson JH, Wolber J, Lipson DA, Lawson R, Wild JM. Direct visualisation of collateral ventilation in COPD with hyperpolarised gas MRI. Thorax. 2012; 67(7):613–617. [PubMed: 22286930]

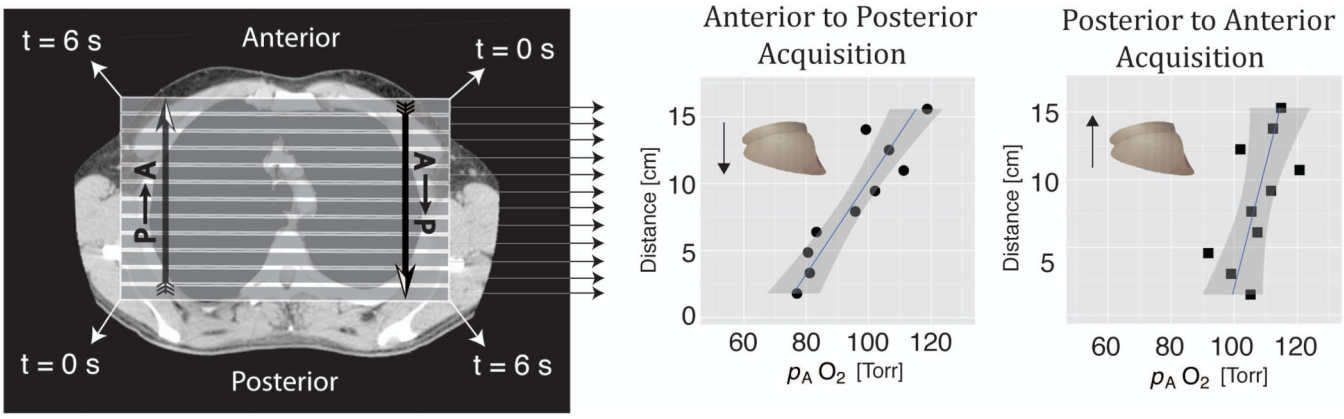

FIGURE 1.

Two separate multislice acquisitions were performed for each subject in two opposite slice order acquisition (anterior slice first A→P, and posterior slice first P→A). Left panel shows a schematic of two sets (A→P and P→A) for 12 slices. It takes about 6 seconds to image the whole lung once from top to bottom (and vice versa). Therefore, the slices that are imaged later will show lower P_AO_2 values due to oxygen uptake during this time. The P_AO_2 extracted from each acquisition is shown on the right panels for each slice (two values for each slice). The two P_AO_2 values evaluated for each identical slice can be averaged to eliminate the effect of different timings for that slice.

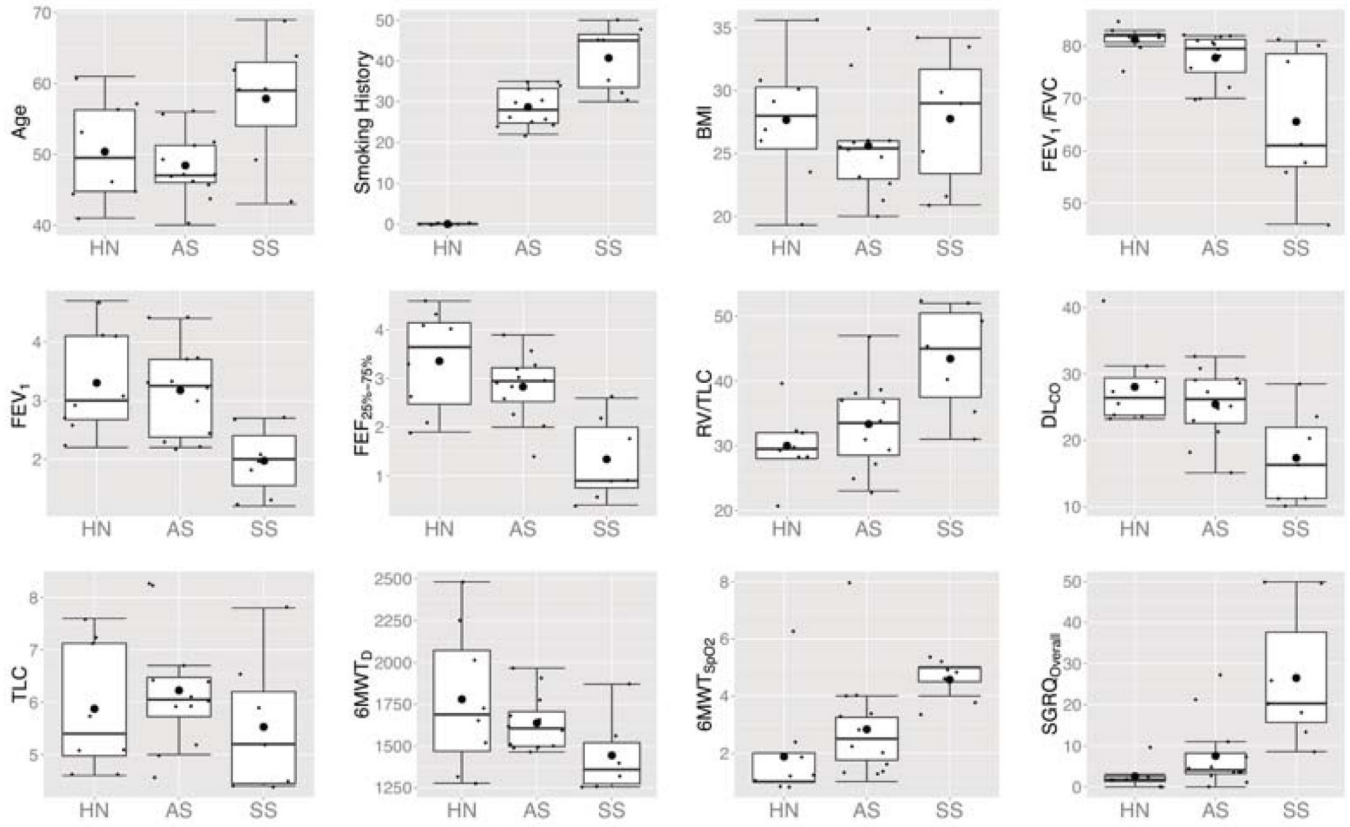

FIGURE 2.

Boxplots representing demographics and a subset of clinical test results (PFT, 6MWT and SGRQ) in all subjects from the three cohorts (healthy nonsmoker, asymptomatic smoker and symptomatic smoker). The middle line in the boxplots shows the median, and the circle shows the mean value for each cohort. The small dots are the individual data for each subject, randomly offset in the horizontal direction for better visibility. The symptomatic (SS) group contains all of the COPD subjects (COPD II-III) as well as smokers with symptoms (COPD-0). The AS group contains smokers with no symptoms, as judged by conventional clinical tests and SGRQ.

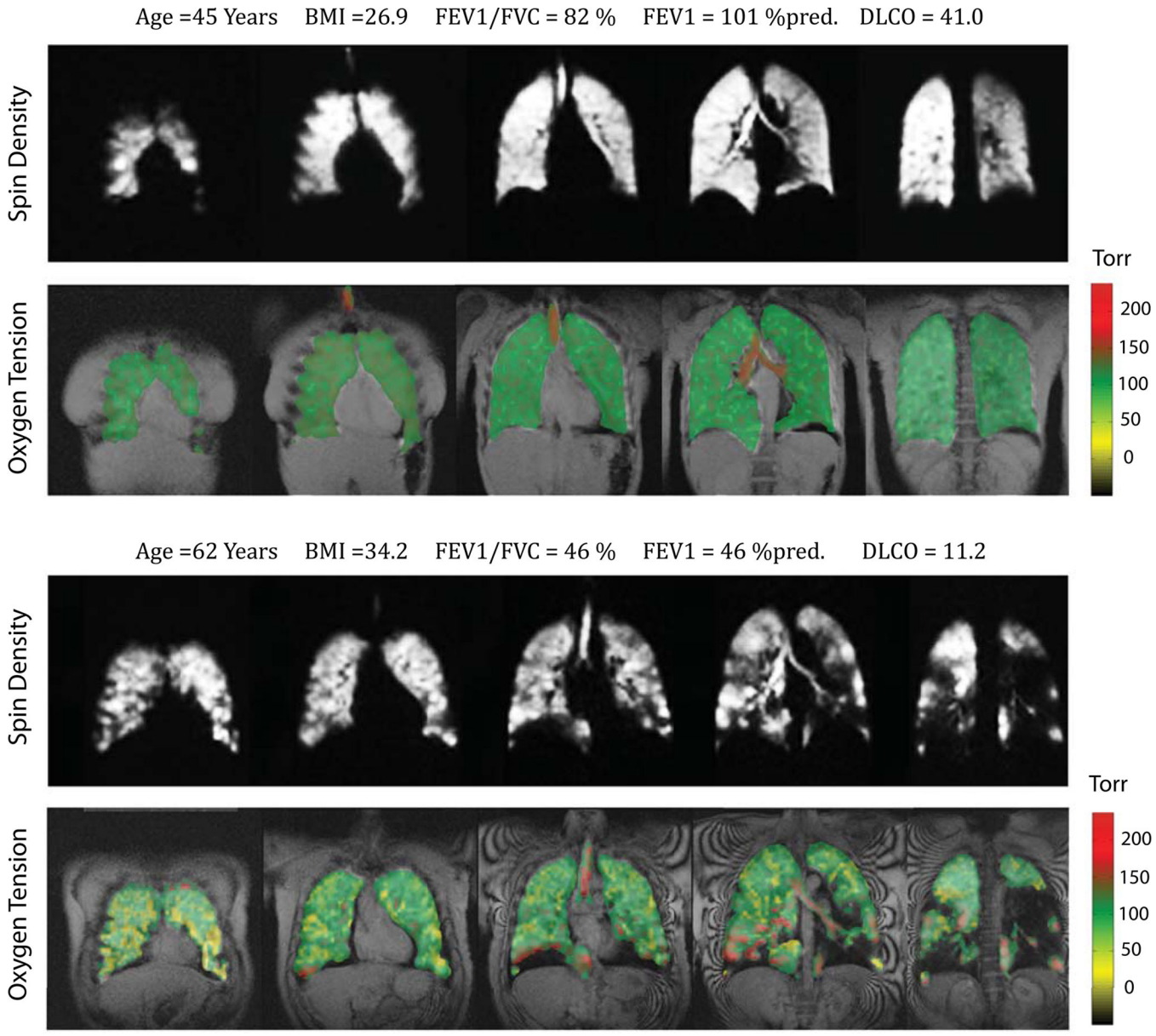

FIGURE 3.

In this figure, ^{3}He spin density for the 1st time-point and the resulting P_AO_2 maps are shown for slices ##2,4,6,8,10. The PFT results and demographics are also shown for comparison. The color maps are designed such that the normal P_AO_2 values near 100 Torr are in green. Voxels in yellow and red show lower and higher values, respectively.

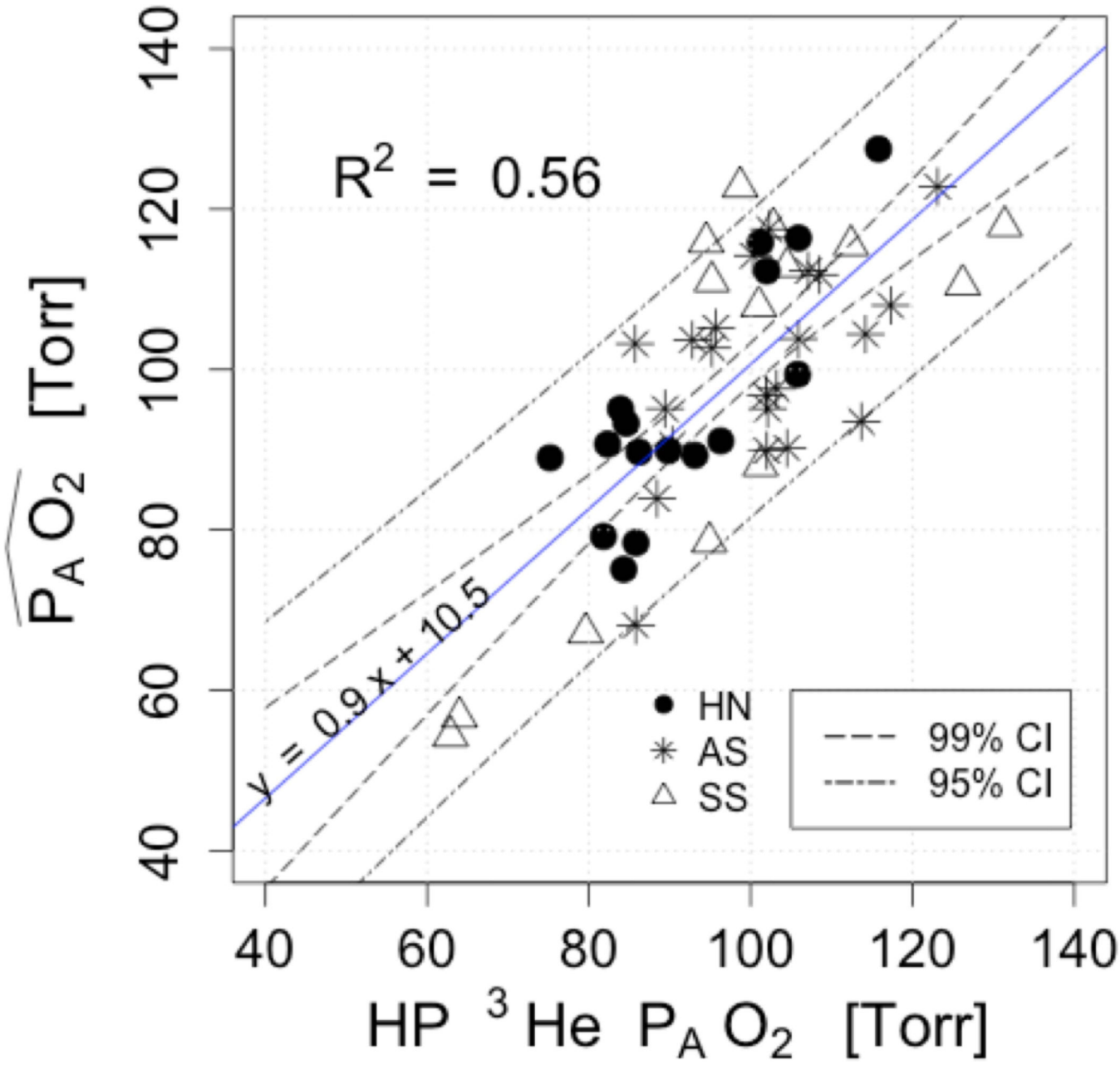

FIGURE 4.

A linear regression to illustrate the association between the imaged global P_AO_2 in each subject and the estimated P_AO_2 based on the end-tidal gas analysis collected from the lung after the 12-second breath-hold. The solid line shows the regression line and the dashed line refers to the 95% and 99% confidence interval. Solid circles are HN, asterisks shows AS and hollow triangles refer to symptomatic subjects.

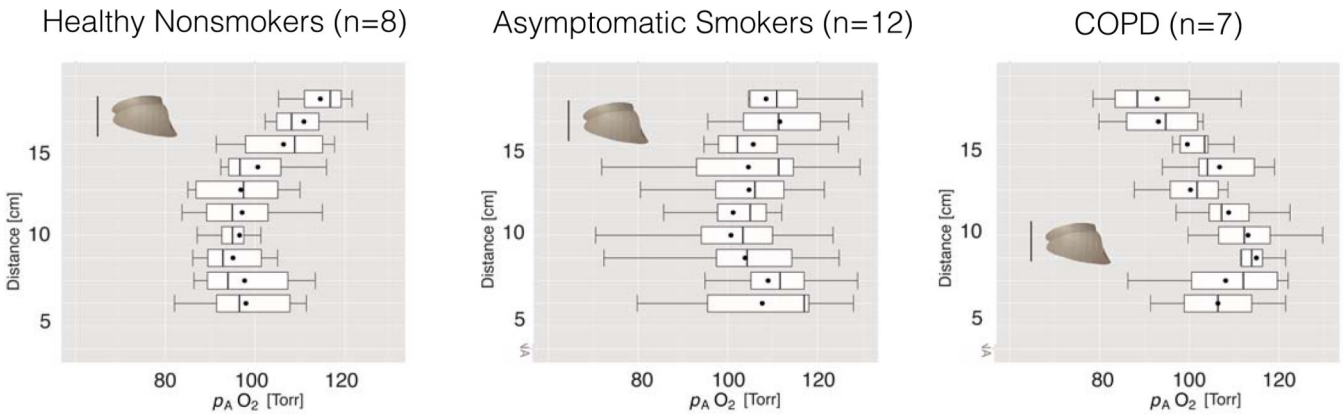

FIGURE 5.

Imaged slice P_AO₂ distribution boxplots for all the subjects from each cohort (healthy nonsmokers, asymptomatic smokers, and symptomatic smokers). Boxplots illustrate the corrected vertical gradients obtained from the average of the identical slice P_AO_2 in the two directions. Each individual box presents the imaged slice P_AO_2 as a function of the distance from the most dependent region of the subject's lung to the anterior slices (from bottom to top). The dot in the boxplot for each slice shows the average, while the line shows the median of the distribution in the entire subject in that cohort.

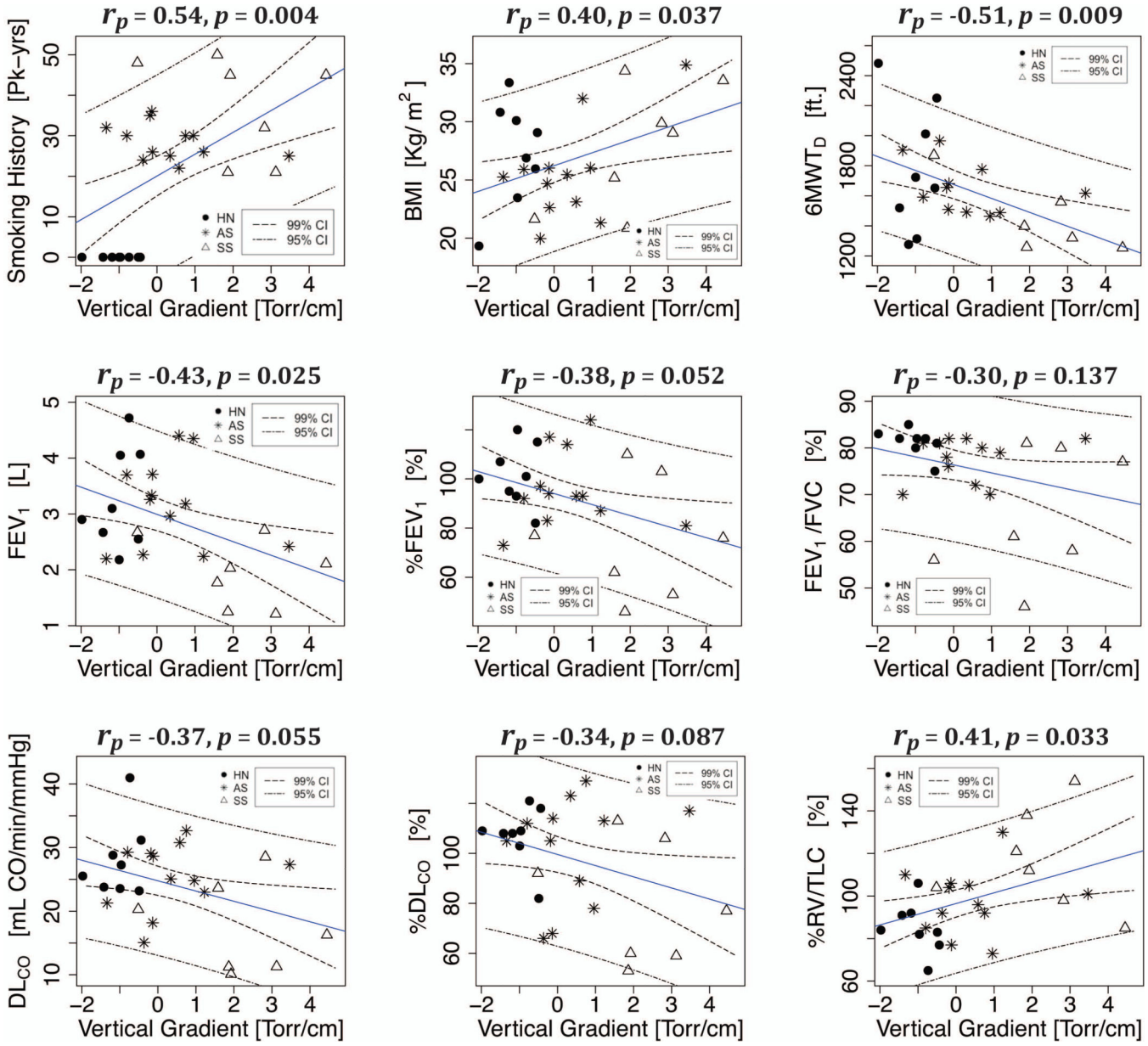

FIGURE 6.

Correlation plots between the vertical gradients and non-imaging metrics. Regression lines are shown by the solid line and 95% and 90% confidence intervals with dashed lines. The solid line shows the regression line and the dashed line refers to the 95% and 99% confidence interval. Healthy nonsmokers are illustrated with solid circles, asymptomatic smokers with asterisks and symptomatic group with hollow triangles.

Table 1

Summary Results of Analysis of Variance for Three Cohorts

	Post Hoc Tukey HSD Test†			
Variables	**Cohorts**	**Mean Diff**	**95% CI***	***p***
Age [Years]	HN-AS	1.96	(−5.74, 9.66)	0.802
	SS-AS	9.44	(1.42, 17.5)	**0.019**
	HN-SS	7.48	(−1.25, 16.2)	0.103
Smoking [Pack-years]	HN-AS	−28.67	(−34.6, −22.8)	**<0.001**
	SS-AS	12.05	(5.89, 18.2)	**<0.001**
	HN-SS	40.71	(34.0, 47.4)	**<0.001**
FEV_1 [Liter]	HN-AS	0.13	(−0.76, 1.01)	0.934
	SS-AS	−1.20	(−2.13, −0.28)	**0.009**
	HN-SS	−1.33	(−2.33, −0.32)	**0.008**
FEV_1/FVC [%]	HN-AS	3.50	(−5.29, 12.3)	0.587
	SS-AS	−12.18	(−21.3, −3.02)	**0.008**
	HN-SS	−15.68	(−25.6, −5.71)	**0.002**
DL_{CO} [ml/min/mmHg]	HN-AS	2.62	(−4.17, 9.41)	0.607
	SS-AS	−8.10	(−15.2, −1.03)	**0.023**
	HN-SS	−10.72	(−18.4, −3.02)	**0.005**
FEV_1, % pred. [%]	HN-AS	5.96	(−13.7, 25.6)	0.733
	SS-AS	−20.38	(−40.9, 0.12)	**0.052**
	HN-SS	−26.34	(−48.6, −4.03)	**0.019**
RV/TLC, % pred [%]	HN-AS	−12.58	(−32.1, 6.93)	0.261
	SS-AS	18.42	(−1.92, 38.8)	0.081
	HN-SS	31.00	(8.87, 53.1)	**0.005**
$6MWT_{Sp\,O2}$	HN-AS	−0.96	(−2.85, 0.94)	0.429
	SS-AS	1.74	(−0.24, 3.71)	0.092
	HN-SS	2.70	(0.55, 4.84)	**0.012**
SGRQ, Overall [%]	HN-AS	−4.97	(−16.7, 6.71)	0.546
	SS-AS	18.94	(6.77, 31.1)	**0.002**
	HN-SS	23.91	(10.7, 37.2)	**<0.001**

*The numbers in the parenthesis shows the 95% confidence interval

†Post Hoc Tukey HSD test was perfomed when the ANOVA test was significant.

AOVA test failed for BMI, TLC and $6MWT_D$: (BMI: F(2, 24) = 0.656, Pr(>F) = 0.528) (TLC: F(2, 24) = 0.760, Pr(>F) = 0.479) ; (6MWTD: F(2, 23) = 2.442, Pr(>F) = 0.109)

Table 2

Summary of Whole-lung Mp_AO_2 and Dp_AO_2 for Each Subject for Both A→P and P→A Directions

ID	*A→P*			*P→A*		
	Mp_AO_2 [torr]	**Dp_AO_2 [torr]**	**ETO_2* [%]**	**Mp_AO_2 [torr]**	**Dp_AO_2 [torr]**	**ETO_2* [%]**
HN-01	102.0	21.0	16.7	101.2	26.7	17.1
HN-02	85.78	20.3	14.6	84.30	26.9	14.3
HN-03	105.9	18.6	17.1	115.8	20.8	18.4
HN-04	84.60	22.4	15.7	75.20	27.8	15.3
HN-05	82.30	28.4	14.4	83.91	39.2	14.9
HN-06	105.8	23.4	15.2	89.84	33.3	14.1
HN-07	96.31	20.2	14.7	93.06	27.8	14.5
HN-08	81.75	27.4	13.3	86.21	30.3	16.3
M±SD	**93.1 ± 10.6**	**22.7 ± 3.5**	**15.2 ± 1.3**	**91.2 ± 12.5**	**29.1 ± 5.4**	**15.6 ± 1.5**
AS-01	62.94	23.2	12.9	64.01	30.9	13.1
AS-02	107.1	29.5	16.7	102.3	33.5	17.3
AS-03	82.15	30.3	-	79.10	32.5	-
AS-04	108.5	41.1	16.5	123.1	24.6	17.8
AS-05	114.2	24.1	16.2	104.5	20.7	14.7
AS-06	79.60	38.3	14.4	101.2	46.7	14.2
AS-07	89.41	26.3	14.7	88.38	26.5	13.4
SS-05	117.3	26.6	16.2	103.2	32.9	15.0
SS-06	102.1	29.8	14.4	113.7	57.6	14.2
AS-08	105.9	33.6	15.7	102.0	45.2	14.1
AS-09	100.3	27.6	17.6	92.81	26.9	16.6
AS-10	95.73	28.3	15.7	95.22	35.5	15.4
M±SD	**97.1 ± 16.0**	**29.9 ± 5.4**	**15.5 ± 1.3**	**97.5 ± 15.5**	**34.5 ± 10.6**	**15.1 ± 1.6**
SS-01	94.53	47.6	17.4	102.8	35.2	17.6
SS-02	85.79	45.9	14.5	85.68	52.7	17.3
SS-03	126.2	55.1	16.7	131.4	69.4	17.5
SS-04	101.0	37.3	17.0	94.86	43.0	14.2

	$A \rightarrow P$			$P \rightarrow A$		
ID	$\mathbf{Mp_AO_2}$ **[torr]**	$\mathbf{Dp_AO_2}$ **[torr]**	$\mathbf{ETO_2}^*$ **[%]**	$\mathbf{Mp_AO_2}$ **[torr]**	$\mathbf{Dp_AO_2}$ **[torr]**	$\mathbf{ETO_2}^*$ **[%]**
SS-07	90.33	49.2	14.3	101.9	39.0	15.0
SS-08	98.67	45.9	17.8	95.2	39.7	16.4
SS-09	112.4	61.8	17.2	104.5	64.4	16.9
M±SD	**101.3 ± 13.9**	**49.0 ± 7.7**	**16.4 ± 1.4**	**102.3 ± 14.3**	**49.0 ± 13.4**	**16.4 ± 1.3**

* Subject AS-03 did not correctly follow the protocol for exhaling into the end-tidal collecting bag.

Table 3

Summary Results of Analysis of Variance for p_AO_2 in Cohorts

		Post Hoc Tukey HSD Test †			
	Variables	**Cohorts**	**Mean Diff**	**95% CI***	***p***
Dp_AO_2	**A→P** [Torr]	HN-AS	−7.19	(−13.6, −0.75)	0.026
		SS-AS	19.07	(12.4, 25.8)	< **0.001**
		HN-SS	26.26	(19.0, 33.6)	< **0.001**
	P→A [Torr]	HN-AS	−5.37	(−17.0, 6.28)	0.493
		SS-AS	14.57	(2.43, 26.7)	**0.017**
		HN-SS	19.94	(6.73, 33.2)	**0.003**

*The numbers in the parenthesis shows the 95% confidence interval

†Post Hoc Tukey HSD test was perfomed when the ANOVA test was significant.

AOVA test failed for Mp_AO_2: (A→P: F(2, 24) = 0.640, Pr(>F) = 0.536) (P→A: F(2, 24) = 1.141, Pr(>F) = 0.336)

Table 4

The Summary of Imaged pAO2 Gradients for all the Subjects

ID	A→P* [Torr/cm]	P→A* [Torr/cm]	Gravity [Torr/cm]
HN-01	−0.06	0.21	−0.44
HN-02	−2.06	0.07	−1.00
HN-03	−1.26	−0.67	−0.96
HN-04	−1.56	−1.27	−1.42
HN-05	−1.84	1.55	−0.74
HN-06	−0.31	−0.68	−0.49
HN-07	−2.86	−1.09	−1.98
HN-08	−2.32	−0.05	−1.18
M ± SD	**−1.53 ± 0.96**	**−0.24 ± 0.90**	**−1.03 ± 0.51**
AS-01	−0.36	1.86	0.75
AS-02	0.61	1.31	0.96
AS-03	−1.68	0.08	−0.80
AS-04	−1.64	−1.04	−1.34
AS-05	−1.78	1.05	−0.37
AS-06	1.42	5.51	3.47
AS-07	−1.35	0.98	−0.18
SS-05	−1.82	1.54	−0.14
SS-06	1.61	0.84	1.22
AS-08	0.10	1.05	0.58
AS-09	−0.90	1.59	0.34
AS-10	−1.73	1.48	−0.12
M ± SD	**−0.63 ± 1.28**	**1.36 ± 1.52**	**0.36 ± 1.22**
SS-01	3.99	−0.14	1.92
SS-02	4.41	1.24	2.83
SS-03	3.21	5.68	4.45
SS-04	1.63	4.61	3.12
SS-05	1.33	1.84	1.59
SS-06	−1.28	0.25	−0.52
SS-07	0.46	3.27	1.86
M ± SD	**1.97 ± 2.04**	**2.39 ± 2.20**	**2.18 ± 1.54**

*Vertical gradients for opposite directions of imaging acquisitions

A: anterior and P: posterior

Table 5

Results of Analysis of Variance for Gradients Among Cohorts

Gradients	Post Hoc Tukey HSD Test †			
	Cohorts	Mean Diff	95% CI*	*p*
A → P [Torr/cm]	HN-AS	−0.91	(−2.54, 0.73)	0.364
	SS-AS	2.59	(0.89, 4.30)	**0.002**
	HN-SS	3.50	(1.64, 5.35)	< **0.001**
P → A [Torr/cm]	HN-AS	−1.60	(−3.40, 0.21)	0.091
	SS-AS	1.04	(−0.85, 2.92)	0.370
	HN-SS	2.63	(0.58, 4.68)	**0.010**
G [Torr/cm]	HN-AS	−1.39	(−2.72, −0.06)	**0.039**
	SS-AS	1.81	(0.43, 3.20)	**0.009**
	HN-SS	3.20	(1.70, 4.71)	< **0.001**

*The numbers in the parenthesis shows the 95% confidence interval

†Post Hoc Tukey HSD test was perfomed when the ANOVA test was significant.